ARTICLE NO. 78-1135

Computation of the Viscous Supersonic Flow over External Axial Corners

Paul Kutler,* Thomas H. Pulliam,† and Yvon C. Vigneron‡
NASA Ames Research Center, Moffett Field, Calif.

The viscous supersonic flowfield surrounding symmetric and asymmetric swept external axial corners is computed using existing second-order, implict and explicit finite-difference computer codes. The governing partial differential equations in conservation-law form are hyperbolic with respect to time and are assumed to be conical; that is, any variation of the radial convective or diffusive terms is assumed to be negligible. An inviscid numerical study for symmetric 90 deg dihedral rounded corners reveals both single and triple crossflow stagnation point flows, depending on the corner radius of curvature. For asymmetrical 90 deg dihedral configurations (i.e., those obtained by varying one of the wedge angles), both single and triple stagnation point flows are also observed. For certain highly asymmetrical configurations, the inviscid flow spills over the corner and in so doing generates a local embedded supersonic bubble. Viscous numerical solutions are obtained for both symmetric and highly asymmetric axial corners for which experimental surface oil flow and vapor screen data are available. For the symmetric configuration, both the laminar and turbulent numerical solutions result in flow away from the corner, which agrees with the experimental data. For the highly asymmetrical configuration, the viscous numerical solution and the experimental data result in flow around the corner. The computed shock locations for both configurations agree fairly well with the experimental vapor screen results.

Introduction

EXTERNAL corners are found on a variety of flight vehicles in existence or in the planning stages. Existing supersonic aircraft, such as the Concorde, F-14, and F-15, possess rectangular engine inlets composed of planar compression or expansion surfaces with swept and unswept leading edges. The configurations of some proposed maneuvering re-entry vehicles and advanced artillery projectiles also possess external corners oriented in the streamwise direction. The occurrence of such corners on flight vehicles can affect its aerodynamic behavior because of the resulting complicated flowfield. To better understand such a flowfield, a simple arrangement of intersecting planar wedges was devised.

A typical external corner configuration of the type studied in this paper, along with some of its associated inviscid flow features, is shown in Fig. 1. The corner is composed of two intersecting wedges with angles δ_1 and δ_2, whose leading edges are swept from the y-z plane at angles Λ_1 and Λ_2. The dihedral of the wedges can be varied by adjusting angles α_1 and α_2, which are measured from the y-z axis bisector. The corner itself is rounded and has a radius of curvature R. Since there is no characteristic length associated with this configuration in the streamwise direction (at least for inviscid flow), the resulting flowfield is conical; that is, independent of the distance along a ray from the conical center.

The exact structure of the inviscid conical flowfield surrounding external corner configurations has been the object of both numerical and experimental research efforts. The problem was first solved numerically by Kutler and Shankar[1] for both symmetric and "slightly" asymmetric configurations (those for which the flow does not circumscribe the corner). The numerical solutions resulted in a triple crossflow stagnation point flowfield: two of the nodal type (or vortical singularity), for which the adjacent flow is toward the stagnation point; and one of the saddle type, for which the adjacent flow is away from the stagnation point. All of the configurations considered possessed equal wedge angles; only the sweep of the leading edges was changed to yield asymmetric shapes. Kutler and Shankar[1] showed that the pressure differential of the two surfaces for the asymmetric configurations was nearly equal, thus precluding the possibility of flow going around the corner.

The first revealing experimental data for both symmetric and "highly" asymmetric configurations (those for which the flow circumscribes the corner) were obtained by Salas and Daywitt[2] and Talcott.[3] Along with their experimental findings, Salas and Daywitt presented a theoretical analysis of the inviscid flow at the corner of a symmetrical configuration based on the irrotational equations. The results of their analysis indicated the possibility of both single and triple crossflow stagnation point flowfields, depending on the external angle Φ (Fig. 1). They showed that for the highly asymmetric configurations, the flow in spilling over the corner must become sonic, then turn through a conical Prandtl-Meyer expansion, and finally, terminate by either an isentropic compression or a shock wave. The primary purpose of the present paper is to verify computationally the experimental results obtained by Salas and Daywitt and shed some light on the process of transition from a triple to a single crossflow stagnation point flowfield.

Figure 2 shows various inviscid flowfields for rounded, sharp, symmetric, and asymmetric configurations. These flowfields are based on the results obtained in the present study, along with the theoretical results of Salas and Daywitt.[2] All cases possess a single peripheral bow shock, whose strength in rounding the corner changes from that of the δ_1-wedge shock to that of the δ_2-wedge shock. The uniform flow region generated by the wedges are bordered on one side by the crossflow sonic line; that is, the locus of points where the crossflow velocity (the component that results when the total velocity is projected on a unit sphere whose focus is

Received July 6, 1978; presented as Paper 78-1135 at the AIAA 11th Fluid and Plasma Dynamics Conference, Seattle, Wash., July 10-12, 1978; revision received Jan. 9, 1979.

Index categories: Computational Methods; Supersonic and Hypersonic Flow; Viscous Nonboundary-Layer Flows.

*Research Scientist, Computational Fluid Dynamics Branch. Associate Fellow AIAA.

†Research Scientist, Computational Fluid Dynamics Branch. Member AIAA.

‡Research Assistant, Iowa State University. Student Member AIAA.

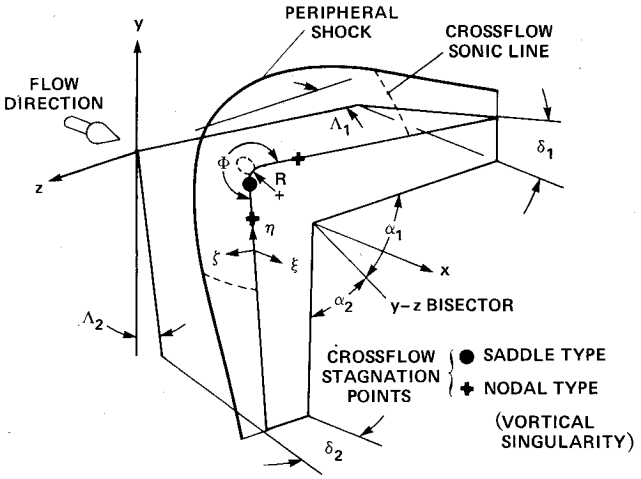

Fig. 1 Coordinate system and flow structure for external axial corner.

at the conical center) is equal to the local speed of sound. The structure of the flow region encompassed by the peripheral shock and crossflow sonic lines depends on whether or not the flow goes around the corner, which, in turn, depends upon the configuration.

For symmetric configurations with highly rounded corners or sharp corners with external angles Φ on the order of (but greater than) π, a single crossflow stagnation point of the nodal type (vortical singularity) exists at the plane of symmetry (Fig. 2a). As the radius of curvature is decreased or Φ is increased, the corner protrudes more into the oncoming flow, thus creating a local pressure maximum (Fig. 2b). This pressure, in turn, forces the flow away from the corner, and, since a crossflow stagnation point must exist at the corner because of symmetry, it results in a triple crossflow stagnation point. The flowfield transition process is probably similar to that occurring on a circular cone when the angle of attack is changed from negative to positive and the vortical singularity moves from one side of the cone to the other.

For asymmetric configurations, both single and triple crossflow stagnation point flowfields are possible. If the single nodal point case of Fig. 2a are made asymmetrical by decreasing the magnitude of the vertical wedge angle (δ_2 in Fig. 1), then that nodal point moves down the surface of the low-pressure wedge. In addition, for the sharp-corner configuration, a local region of embedded supersonic crossflow forms, as explained earlier (see also Chattot[4]).

If, initially, a triple crossflow stagnation point flowfield exists and again asymmetry is introduced by decreasing the vertical wedge angle, the resulting structure of the conical flowfield depends solely on the degree of this asymmetry. The transition process from a triple to a single crossflow stagnation point structure for the sharp corner is moot, but it could easily be resolved with further numerical experiments.

Decreasing the vertical wedge angle for the rounded corner configuration causes the nodal point of the high-pressure wedge and the saddle point to coalesce on the corner (see the left side of Figs. 2d and 2e). To accomplish this, the vertical wedge angle must be decreased sufficiently to first overcome the local pressure maximum existing at the saddle point. Once this occurs, the crossflow still decelerates near the region, but never actually stagnates. It then rapidly accelerates around the corner, decelerates, and finally stagnates in the crossflow plane at the nodal point on the low-pressure wedge.

For the sharp-corner configuration, two possible flowfields are hypothesized to explain the transition (see the right side of Figs. 2d and 2e); either, or possibly both, can occur during the transition process. In the first hypothetical model, as the vertical wedge angle is decreased, the nodal point on the horizontal wedge coalesces with the saddle point, which

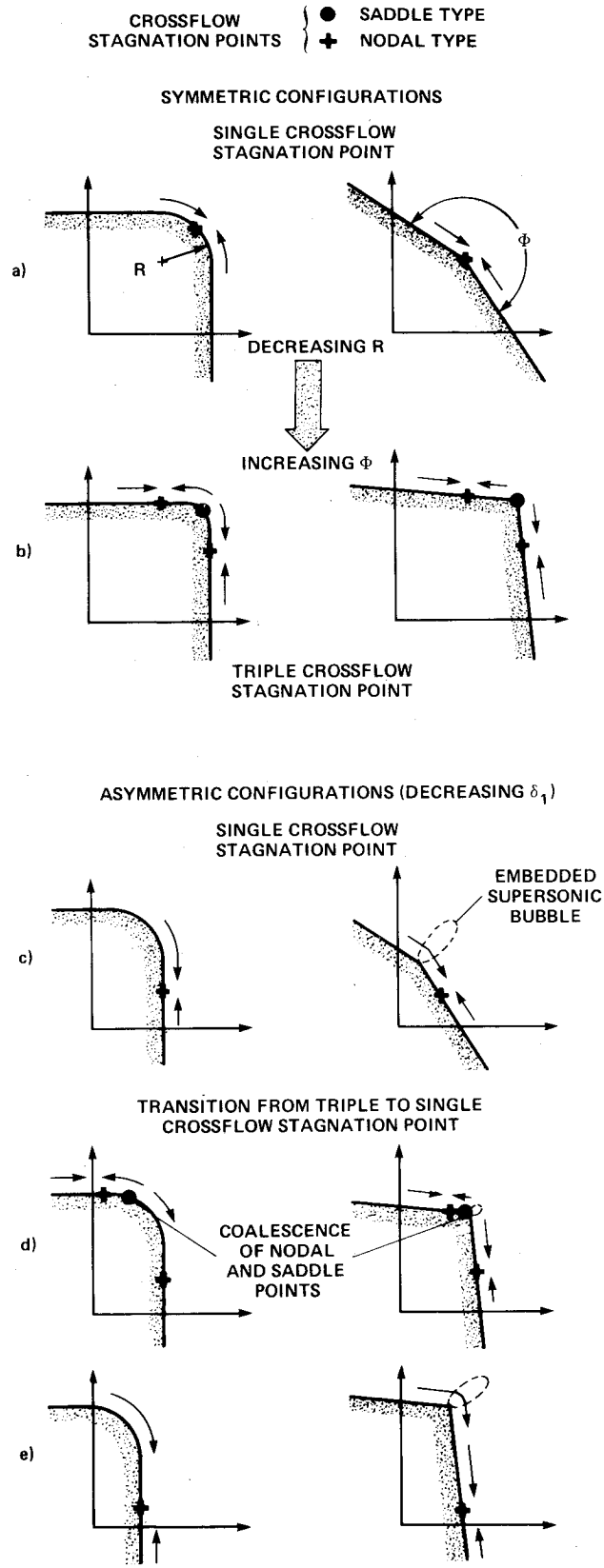

Fig. 2 Scenario of possible flowfields for external axial corners.

remains fixed at the sharp corner. After this occurs, the flow then spills over the corner, causing the embedded supersonic bubble to form. The single crossflow stagnation point flowfield is thus established.

In the second hypothetical model, coalescence of the horizontal nodal point and the saddle point again occurs with

a decreasing vertical wedge angle; but, in this case, the saddle point moves away from the corner. The flow immediately begins to spill over the sharp corner, resulting in a small embedded supersonic bubble, which become larger as more asymmetry is introduced. A determination of the correct transition model is planned for the future.

Governing Equations

Two existing computer codes were used to compute the supersonic flowfield surrounding the external axial corner. For the inviscid and turbulent flow results, the unsteady, three-dimensional implicit code of Pulliam and Steger[5] was used; its adaptation to the present problem is described in detail later. For the laminar flow results, the unsteady two-dimensional explicit procedure of Vigneron et al.[6] was used. This code, originally designed to determine the viscous flow about subsonic edge delta wings, is explained in Vigneron's paper. The implicit code is based on the shock-capturing philosophy, while the explicit code uses a sharp shock philosophy. Both codes are second-order accurate in space and solve the conservation-law form of the governing partial differential equations.

Equations in Nondimensional Form

For the inviscid and turbulent calculations, the three-dimensional unsteady "thin layer" Navier-Stokes equations in an arbitrary curvilinear coordinate system (ξ,η,ζ,τ) are used (see Pulliam and Steger[5]). The equations in strong conservation-law form retain their inertial Cartesian velocity components and readily absorb arbitrary geometrical transformations. For the axial corner problem, the governing thin-layer equations also are assumed to be conical (McRae[7]); hence, variations of the radial convective or diffusive terms are neglected. Under the assumption of conicity, the Cartesian coordinates can be written as:

$$x=\xi, \quad y=\xi y^0(\eta,\zeta), \quad z=\xi z^0(\eta,\zeta) \tag{1}$$

The functions y^0 and z^0, which describe the mesh, will be defined later.

The thin-layer equations under the preceding assumptions reduce to:

$$U_\tau+F_\eta+G_\zeta+H=S_\zeta/Re \tag{2}$$

$$U=J^{-1}\begin{bmatrix}\rho\\ \rho u\\ \rho v\\ \rho w\\ e\end{bmatrix} \qquad F=J^{-1}\begin{bmatrix}\rho V\\ \rho uV+\eta_x P\\ \rho vV+\eta_y P\\ \rho wV+\eta_z P\\ (e+P)V\end{bmatrix}$$

$$G=J^{-1}\begin{bmatrix}\rho W\\ \rho uW+\zeta_x P\\ \rho vW+\zeta_y P\\ \rho wW+\zeta_z P\\ (e+P)W\end{bmatrix}$$

$$H=\frac{2}{\xi}J^{-1}\begin{bmatrix}\rho u\\ \rho u^2+P\\ \rho uv\\ \rho uw\\ (e+P)u\end{bmatrix}$$

$$S=J^{-1}\begin{bmatrix}0\\ \mu(\zeta_x^2+\zeta_y^2+\zeta_z^2)u_\zeta\\ \quad+(\mu/3)(\zeta_x u_\zeta+\zeta_y v_\zeta+\zeta_z w_\zeta)\zeta_x\\ \mu(\zeta_x^2+\zeta_y^2+\zeta_z^2)v_\zeta\\ \quad+(\mu/3)(\zeta_x u_\zeta+\zeta_y v_\zeta+\zeta_z w_\zeta)\zeta_y\\ \mu(\zeta_x^2+\zeta_y^2+\zeta_z^2)w_\zeta\\ \quad+(\mu/3)(\zeta_x u_\zeta+\zeta_y v_\zeta+\zeta_z w_\zeta)\zeta_z\\ \{(\zeta_x^2+\zeta_y^2+\zeta_z^2)[0.5\mu(u^2+v^2+w^2)_\zeta\\ \quad+\kappa Pr^{-1}(\gamma-1)^{-1}(a^2)_\zeta]+(\mu/3)\\ \times(\zeta_x u+\zeta_y v+\zeta_z w)(\zeta_x u_\zeta+\zeta_y v_\zeta+\zeta_z w_\zeta)\}\end{bmatrix}$$

where $V=\eta_x u+\eta_y v+\eta_z w$ and $W=\zeta_x u+\zeta_y v+\zeta_z w$.

The Cartesian velocity components are nondimensionalized with respect to a_∞ (the freestream speed of sound); density ρ is referenced to ρ_∞ and total energy e to $\rho_\infty a_\infty^2$. The pressure, density, and velocity components are related to the total energy by the following equation for an ideal gas:

$$p=(\gamma-1)[e-(\rho/2)(u^2+v^2+w^2)] \tag{3}$$

where γ is the ratio of specific heats (taken as 1.4). Also, μ is the dynamic viscosity, Re is the Reynolds number, and Pr is the Prandtl number.

In Eq. (1), the geometric factors (metrics) resulting from the conical coordinate transformation are defined as follows in terms of the derivatives of the Cartesian coordiantes of the nodal points:

$$\left.\begin{aligned}&\eta_x=\xi(z^0y^0_\zeta-y^0z^0_\zeta)J \qquad \eta_y=\xi z^0_\zeta J\\ &\eta_z=-\xi y^0_\zeta J \qquad \zeta_x=\xi(y^0z^0_\eta-z^0y^0_\eta)J\\ &\zeta_y=-\xi z^0_\eta J \qquad \zeta_z=\xi y^0_\eta J\end{aligned}\right\} \tag{4}$$

where

$$J^{-1}=\xi^2(y^0_\eta z^0_\zeta-y^0_\zeta z^0_\eta)$$

Thin-Layer Approximation

The thin-layer approximation of the Navier-Stokes equations is most applicable to high Reynolds number flows where viscous effects are usually restricted to a thin region near a solid boundary. Typically, computer storage is available for only enough grid points to resolve the viscous terms in the direction nearly normal to the body (those of most importance). Numerical resolution is so coarse along the body that the viscous derivatives in that direction may as well be neglected. Hence, in the thin-layer approximation, all the viscous derivatives along the body (i.e., in both the ξ and η directions) are dropped from the equations, while those in the ζ direction (Fig. 1) are retained. This assumes, of course, that the body conforms to a ζ = constant surface. The applicability of the thin-layer equations for computing attached and separated boundary-layer flows has been demonstrated by Baldwin and Lomax,[8] Steger,[9] and Pulliam and Steger.[5]

Viscous Models

Inviscid results are presented along with viscous laminar calculations which use Sutherland's law for the laminar viscosity coefficient. For the turbulent cases, an algebraic eddy viscosity turbulence model of the Cebeci-type devised by Baldwin and Lomax[8] is used.

Surface Boundary Conditions

The tangency condition at the body surface where $\zeta(x,y,z,t) = \text{const}$ for inviscid flow is $W=0$. This, in conjunction with the following equation, yields the inertial velocity components:

$$\begin{pmatrix} v \\ w \end{pmatrix} = J^{-1} \begin{vmatrix} -(\eta_x\zeta_z - \eta_z\zeta_x) & \zeta_z & -\eta_z \\ (\eta_x\zeta_y - \eta_y\zeta_x) & -\zeta_y & \eta_y \end{vmatrix} \begin{pmatrix} u \\ V \\ W \end{pmatrix} \quad (5)$$

For viscous flows, the conditions $u=V=W=0$ are used in Eq. (5).

When the three momentum equations are combined, a normal momentum equation can be formed and used to obtain pressure at the surface

$$(\eta_x\zeta_x + \eta_y\zeta_y + \eta_z\zeta_z)P_\eta + (\zeta_x^2 + \zeta_y^2 + \zeta_z)P_\zeta = \rho[(\zeta_t)_\tau + u(\zeta_x)_\tau + v(\zeta_y)_\tau + w(\zeta_z)_\tau] - \rho V(\zeta_x u_y + \zeta_y v_y + \zeta_z w_z) \quad (6)$$

The same relation is used with $u=V=0$ for viscous flows.

Numerical Method

The conical equations are solved with an implicit, approximate factorization, finite-difference algorithm. The basic algorithm is described in detail by Beam and Warming.[10] For the sake of brevity, the equations of the algorithm are omitted, and just some of the characteristics of the scheme will be discussed.

An implicit method was chosen to avoid restrictive stability conditions that may occur when small grid spacings are used for accuracy or viscous resolution. The approch used here is to relax in time the unsteady equations to the steady-state solution. The implicit method allows the use of large time steps for this purpose.

The basic algorithm is first-order accurate in time, noniterative, and in the so-called "delta form," that is, the equations are solved for ΔU as opposed to U. The Jacobian matrices of the time linearizations of the flux vectors (F and G) and the viscous vector S are the same as presented by Pulliam and Steger.[5] The equations are factored, which reduces the solution process to two one-dimensional operators at a given time level. Fourth order central differences are used for the convective derivatives on the right-hand side of the algorithm, which produces fourth-order accuracy in the steady state. Second-order central differences are used for all the remaining derivatives. The source term is added explicitly and does not affect the stability of the scheme. Second- and fourth-order dissipations are added to control possible nonlinear instabilities.

Numerical Implementation of Boundary Conditions

Unknown values of U at the boundaries are updated explicitly and ΔU is set equal to zero, resulting in a first-order error in time which vanishes as the steady state is approached.

For inviscid flows, values of ρ, u, and V along the body are extrapolated from the points directly above the body, while for viscous flows, u and V are set equal to zero. In either case, Eq. (5) is solved for v and w on the body. Pressure P is found from the numerical integration of Eq. (6), and total energy is then obtained from Eq. (3). Freestream conditions are held constant at the outer boundary, while at the side boundaries, supersonic in-flow conditions are imposed.

Mesh Generation

The two-dimensional computational mesh is generated by distributing points in the ζ-direction between the body and an outer boundary, which is chosen to lie beyond the peripheral bow shock. For inviscid computations, the points are linearly distributed between these two boundaries, while for viscous solutions they are heavily clustered near the body using an exponential function.

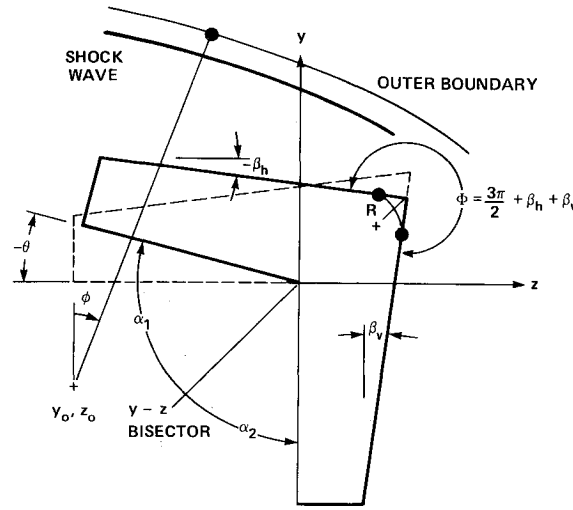

Fig. 3 Body geometry and mesh generation.

The equations describing the horizontal and vertical wedge surfaces (Fig. 3) for use in Eq. (1) are as follows:

$$y = [z\sin\theta_1 + (x + z\cos\theta_1\tan\Lambda_1)\tan\delta_1]/[\cos\theta_1 - \sin\theta_1\tan\Lambda_1\tan\delta_1] \quad (7)$$

for horizontal wedge where

$$\theta_1 = \pi/4 - \alpha_1$$

and

$$z = [y\sin\theta_2 + (x + y\cos\theta_2\tan\Lambda_2)\tan\delta_2]/[\cos\theta_2 - \sin\theta_2\tan\Lambda_2\tan\delta_2] \quad (8)$$

for vertical wedge where

$$\theta_2 = \pi/4 - \alpha_2$$

The slopes of the wedge surfaces in the y-z plane at $x=1$ are found from the following expressions:

$$\beta_h = \tan^{-1}(dy/dz)_h \quad \text{for horizontal wedge} \quad (9)$$

$$\beta_v = \tan^{-1}(dz/dy)_v \quad \text{for vertical wedge} \quad (10)$$

For the rounded-corner configurations, a circular arc of radius R (Fig. 3) is placed at the corner, such that continuity of the body slope is maintained.

The flowfield in the η direction, that is, along the body, is discretized by radial lines that are rotated between $\phi_{\min}$ and $\phi_{\max}$ about a common point (y_0,z_0) (see Fig. 3). The angle $\phi_{\min}$ is chosen to lie to the left of the crossflow sonic line on the horizontal wedge, and $\phi_{\max}$ is chosen to lie below the crossflow sonic line on the vertical wedge. The radial lines are clustered in the vicinity of the corner.

Numerical Results

For both symmetric and asymmetric configurations, numerical solutions are presented that exhibit both single and triple crossflow stagnation point flowfields. A typical inviscid solution required 500 iterations and approximately 3-1/2 min of CDC-7600 computer time to converge. The computational mesh consisted of 15 points between the body and outer boundary and 49 points around the body. The laminar flow solutions obtained by Vigneron used a 30×35 grid, required approximately 2000 iterations to converge, and consumed

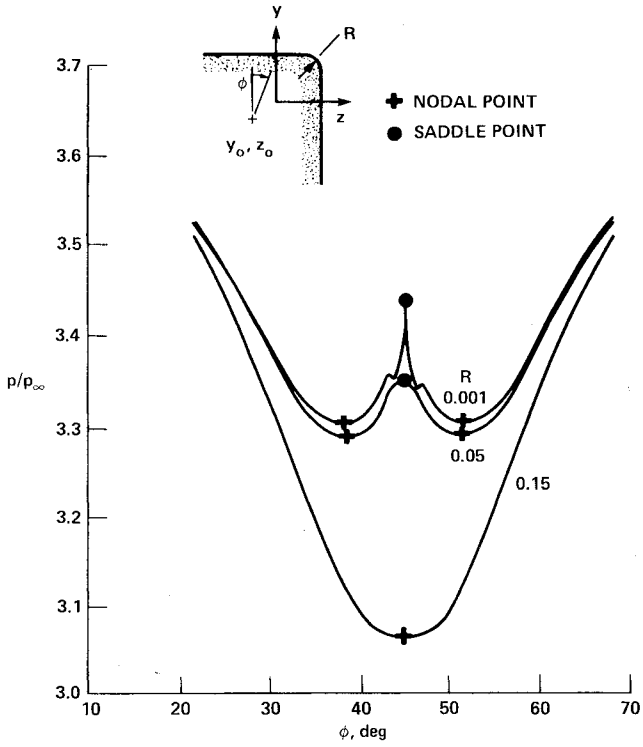

Fig. 4 Variation of surface pressure distribution with corner radius: $M_\infty = 6$, $\delta_1 = \delta_2 = 10$ deg, $\Lambda_1 = \Lambda_2 = -30$ deg, $\alpha_1 = \alpha_2 = 45$ deg, $y_0 = z_0 = -0.34$.

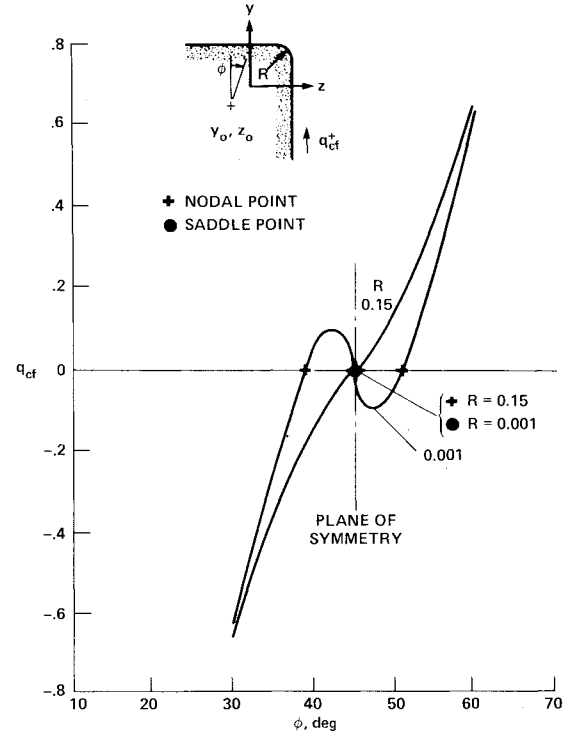

Fig. 5 Surface crossflow velocity for single and triple stagnation point symmetric flows: $M_\infty = 6$, $\delta_1 = \delta_2 = 10$ deg, $\Lambda_1 = \Lambda_2 = -30$ deg, $\alpha_1 = \alpha_2 = 45$ deg, $y_0 = z_0 = -0.34$.

about 9 min of computer time. The turbulent flow results which used the implicit code used a 30×39 grid and required 8 min of computer time for convergence.

To study the transition process from a single to a triple-crossflow stagnation point flowfield structure for rounded corners (Figs. 2a and 2b), a symmetric configuration con-

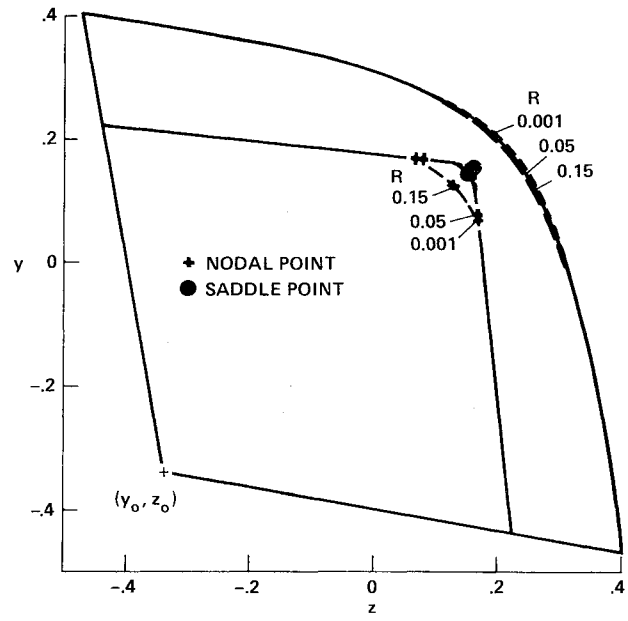

Fig. 6 Variation of shock shape and crossflow stagnation point locations with corner radius: $M_\infty = 6$, $\delta_1 = \delta_2 = 10$ deg, $\Lambda_1 = \Lambda_2 = -30$ deg, $\alpha_1 = \alpha_2 = 45$ deg, $y_0 = z_0 = -0.34$.

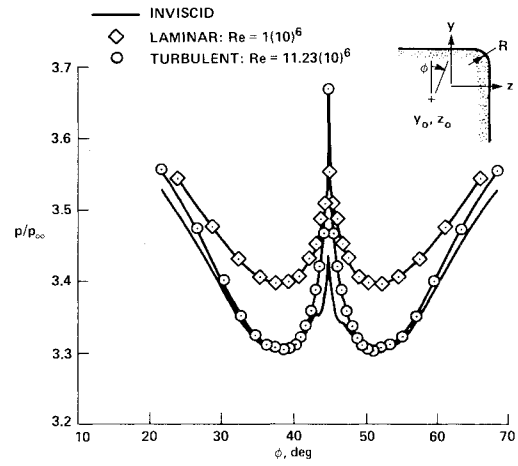

Fig. 7 Surface pressure distribution near corner: $M_\infty = 6$, $\delta_1 = \delta_2 = 10$ deg, $\Lambda_1 = \Lambda_2 = -30$ deg, $\alpha_1 = \alpha_2 = 45$ deg, $y_0 = z_0 = -0.34$, $R = 0.0001$.

sisting of 10 deg wedges, each with -30 deg leading-edge sweep, was computationally tested. The corner radius R was varied from 0.15 to 0.001; the freestream Mach number was 6. Except for the rounded corner, these conditions are identical to those of the experiment performed at Langley Research Center.[2,3] The inviscid results of this study are shown in Figs. 4-6.

The surface pressure distribution for three different corner radii is shown in Fig. 4. For the large corner radius ($R = 0.15$), a single crossflow stagnation point of the nodal type (vortical singularity) exists at the plane of symmetry, as can be observed in the surface crossflow velocity plot of Fig. 5. The pressure reaches a local minimum there and has a zero pressure gradient. As the corner radius is decreased (or, in turn, as the corner is extended more into the oncoming flow), the pressure at the plane of symmetry increases and eventually a local maximum occurs ($R = 0.05$). This forces the flow away from the corner and results in the triple crossflow stagnation point structure. For a corner radius of 0.001, the pressure distribution near the plane of symmetry approaches the cusp-like behavior predicted by the analysis of Salas and Daywitt[2] for sharp corners. However, even for slightly rounded cor-

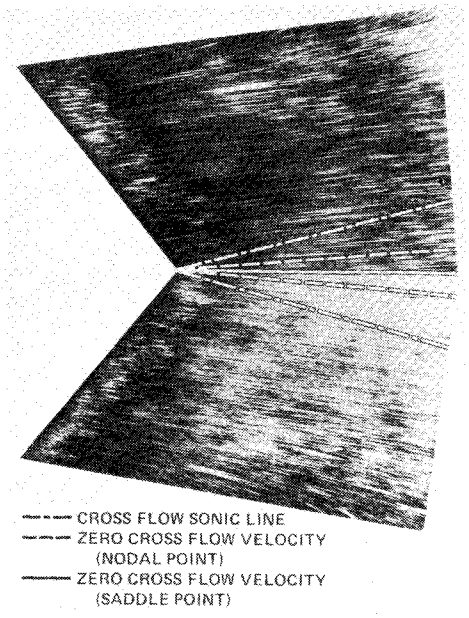

Fig. 8 Oil streaklines on symmetric model: $M_\infty = 6$, $\delta_1 = \delta_2 = 10$ deg, $\Lambda_1 = \Lambda_2 = -30$ deg, $\alpha_1 = \alpha_2 = 45$ deg.

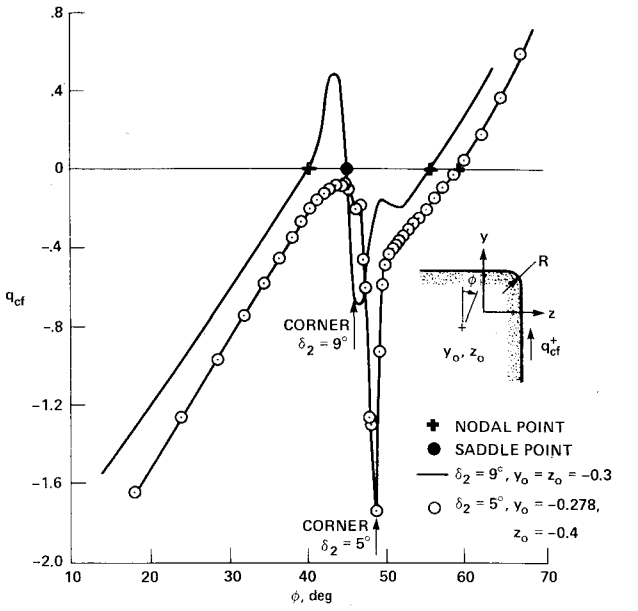

Fig. 10 Surface crossflow velocity for asymmetric configurations: $M_\infty = 6$, $\delta_1 = 10$ deg, $\Lambda_1 = -30$ deg, $\Lambda_2 = 30$ deg, $\alpha_1 = \alpha_2 = 45$ deg, $R = 0.001$.

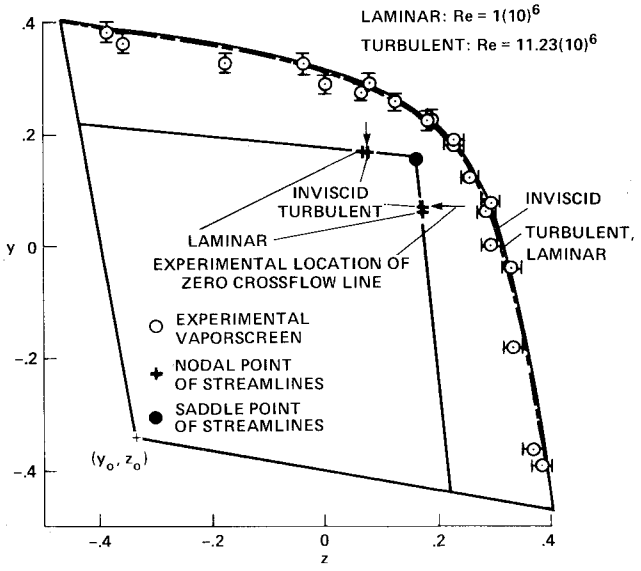

Fig. 9 Shock shape and near-surface crossflow stagnation point locations: $M_\infty = 6$, $\delta_1 = \delta_2 = 10$ deg, $\Lambda_1 = \Lambda_2 = -30$ deg, $\alpha_1 = \alpha_2 = 45$ deg, $y_0 = z_0 = -0.34$, $R = 0.001$, $Re_{lam} = 1(10)^6$, $Re_{tur} = 11.23(10)^6$.

ners, the pressure gradient is still zero right at the plane of symmetry. It is the lack of computational nodal points that simply fails to disclose this flow feature. However, a more predominant triple crossflow stagnation point flowfield exists for this smaller corner radius solution. Thus, it would seem impossible that for a truly sharp corner, with all of the other same geometrical specifications, a flowfield with a single crossflow stagnation point of the nodal type could exist as Salas and Daywitt suggest.

The geometry, shock shape, and crossflow stagnation point locations for the three different corner radii are shown in Fig. 6. As can be observed, the corner radius has a very minimal effect on the shock shape. However, as shown in Fig. 6 for the triple crossflow stagntion point flows, as the corner radius decreases, the nodal points tend to move further from the corner.

Both laminar and turbulent boundary-layer computational results were obtained for the $R = 0.001$ symmetric configuration. For the laminar case, a constant temperature wall was assumed; while for the turbulent case, an adiabatic wall condition was imposed.

Figure 7 compares the surface pressure distribution for both viscous solutions and the inviscid result. Both viscous results exhibit a local maximum in the pressure at the plane of symmetry and local minimums on either side of the corner, as does the inviscid result. As expected, the near-surface crossflow velocities for these viscous results show the flow going away from the corner and stagnating in the crossflow plane where the local pressure minimum occur, as seen in Fig. 7.

Figure 8 shows a composite photograph of the two sides of the experimental oil flow for the symmetric configuration. The smooth behavior of the flow indicates the absence of dominating viscous effects. The locations of the three crossflow stagnation points are indicated by a dashed line for the nodal type (i.e., flow toward this point), and a solid line for the saddle-type (i.e., flow away from this point). Also shown is the approximate location of the crossflow sonic line. In this photograph, an angle of approximately 5 deg occurs between the saddle point and nodal point of the streamlines. The equivalent angle determined from the computational results for the inviscid and turbulent boundary-layer cases is 4.9 deg.

The computed peripheral shock shape for the inviscid, laminar, and turbulent cases is shown in Fig. 9. Superimposed on this figure are the experimental data points with error bars obtained from the vapor screen results. Also shown is the approximate experimental location of the zero crossflow line. The computational solutions and experimental results all seem to be in good agreement for the inviscidly dominated symmetric case.

A sequence of asymmetric configurations was tested to demonstrate the existence of both single and triple crossflow stagnation point flowfields. The geometrical properties consisted of a 10 deg horizontal wedge swept forward 30 deg and a vertical wedge whose angle was varied but whose sweep was fixed at -30 deg. The corner radius was $R = 0.001$ at $x = 1$. Inviscid results for the 5 and 9 deg vertical wedges in the form of surface crossflow velocity plots are shown in Fig. 10. The 9 deg asymmetric solution clearly yields a triple crossflow stagnation point flowfield. As noted on this figure, the saddle point occurs first to the left of the slightly rounded corner.

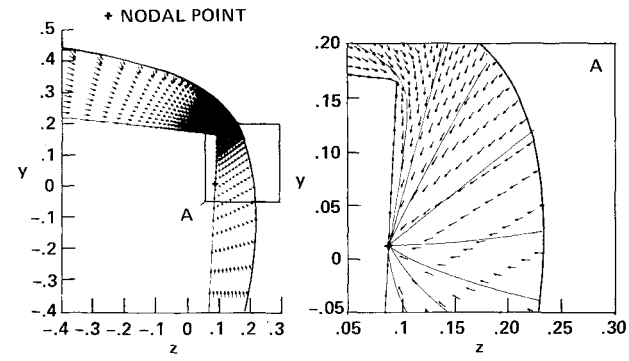

Fig. 11 Crossflow velocity vectors for highly asymmetrical configuration: $M_\infty = 6$, $\alpha_1 = 10$ deg, $\alpha_2 = 5$ deg, $\Lambda_1 = -30$ deg; $\Lambda_2 = 30$ deg, $\alpha_1 = \alpha_2 = 45$ deg.

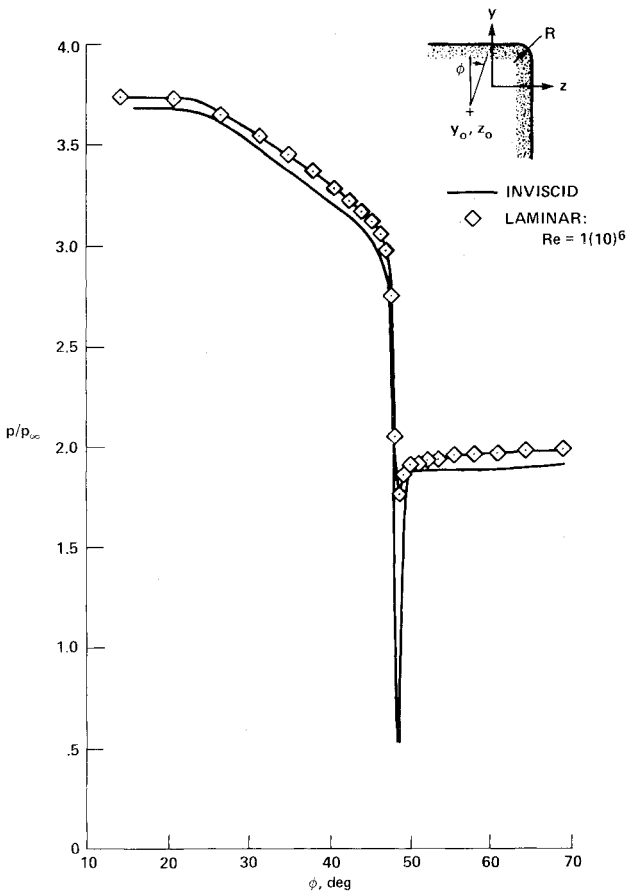

Fig. 12 Surface pressure distribution near corner for highly asymmetrical configuration: $M_\infty = 6$, $\delta_1 = 10$ deg, $\delta_2 = 5$ deg, $\Lambda_1 = -30$ deg, $\Lambda_2 = 30$ deg, $\alpha_1 = \alpha_2 = 45$ deg, $y_0 = -0.278$, $z_0 = -0.4$, $R = 0.001$.

Transition from a triple to a single crossflow stagnation point field occurs between the 8 deg and 9 vertical wedge angle configurations.

The inviscid result for the 5 deg vertical wedge angle shape is also shown in Fig. 10. The actual computational points are plotted to indicate the spacing. The crossflow velocity decelerates while passing through the crossflow sonic line and reaches a local minimum but it never stagnates. As the flow approaches the corner, it accelerates. In rounding the corner, the flow becomes supersonic and then decelerates to subsonic velocity. Proceeding down the vertical wedge, the crossflow finally stagnates at the only stagnation point—a vortical singularity.

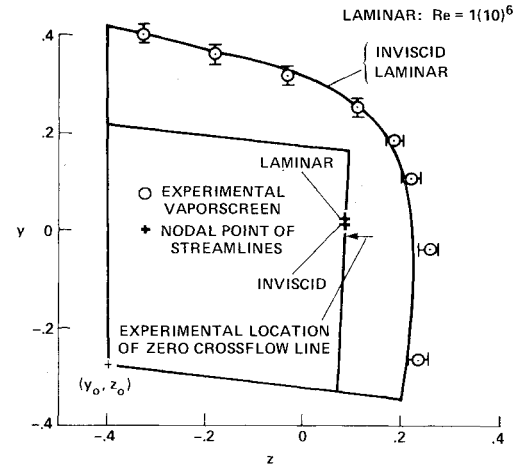

Fig. 13 Shock shape and near-surface crossflow stagnation point location: $M_\infty = 6$, $\delta_1 = 10$ deg, $\delta_2 = 5$ deg, $\Lambda_1 = -30$ deg, $\Lambda_2 = 30$ deg, $\alpha_1 = \alpha_2 = 45$ deg, $y_0 = -0.278$, $z_0 = -0.4$, $R = 0.001$.

Figure 11 shows a computer-generated plot of the inviscid crossflow velocity vectors for the computational region and clearly shows the flow spilling over the corner and stagnating on the vertical wedge.

A laminar viscous solution was generated for this same highly asymmetric case. Figure 12 compares the surface pressure distribution and the inviscid solution. The viscous solution considerably reduces the spike in the pressure that occurs as a result of the flow spilling over the corner. The pressure distribution from the laminar solution on the vertical wedge is slightly higher than that of the inviscid solution, which is probably a result of the apparent thickening of the body by the boundary layer.

The crossflow velocities in the vicinity of the corner indicate a thin region of separated flow on the low-pressure wedge just aft of the corner. However, no massive separation bubble is observed. The crossflow velocity vectors are quite similar to those of the inviscid flow.

Figure 13 compares the computed shock shape with the shock shape obtained from the experimental vapor screen study. The agreement is seen to be good on the horizontal (high pressure) wedge but not so good on the vertical (low-pressure) wedge. This is probably a result of the large separation bubble that occured near the surface of the vertical wedge.

Also shown in Fig. 13 are the computed and experimental locations of the single crossflow stagnation point. The experimental location is slightly further down the side of the vertical wedge.

Conclusions

Both viscous and inviscid numerical solutions have been obtained for the supersonic flowfield surrounding symmetric and asymmetric swept external, conical axial corners. Existing explicit and implicit, second-order, finite-difference computer codes were employed.

Inviscid solutions for a symmetric configuration with a rounded corner resulted in either single or triple surface crossflow stagnation point flows, depending on the corner radius. Numerical results obtained for the same symmetric configuration tested experimentally show the crossflow in the vicinity of the corner to be away from the corner (triple crossflow stagnation point structure) and thus in agreement with the experimental oil flow results.

It has been demonstrated numerically that for asymmetric configurations with slightly rounded corners, both single and triple crossflow stagnation point flows are possible. For highly asymmetric configurations, the flow spills over the

corner and in so doing, undergoes a conical analog of a Prandtl-Meyer expansion, followed by a rapid compression as suggested by Salas and Daywitt. However, it cannot be deduced from the present numerical results whether or not an isentropic compression or shock wave occurred near the corner. Again, the numerical solution agreed fairly well with the oil flow and vapor screen results for this particular asymmetric configuration.

Acknowledgments

The authors thank the NASA-Ames University Consortium Office and the Iowa State University Engineering Research Institute for partial support of this work. In addition, the authors thank M. Salas and J. Daywitt, and N. Talcott Jr., NASA Langley Research Center, for providing the detailed experimental data and many helpful discussions.

References

[1]Kutler, P. and Shankar, V., "Computation of the Inviscid Supersonic Flow Over an External Axial Corner," *Proceedings of the the 1976 Heat Transfer and Fluid Mechanics Institute*, Davis, Calif., June 1976, pp. 356-373.

[2]Salas, M. D. and Daywitt, J., "Structure of the Conical Flow Field About External Axial Corners," AIAA Paper 78-59, Huntsville, Ala., Jan. 1978, submitted to *AIAA Journal*.

[3]Talcott, N. A., "Field Visualization About External Axial Corners," NASA TM 78682, March 1978.

[4]Chattot, Jean-Jacques, "Symmetrical Flow Past a Double Wedge at High Subsonic Mach Number," Rept. No. AS-71-3, Aeronautical Sciences Division, University of California, June 1971.

[5]Pulliam, T. H. and Steger, J. L., "On Implicit Finite-Difference Simulations of Three-Dimensional Flow," AIAA Paper 78-10, Huntsville, Ala., Jan. 1978.

[6]Vigneron, Y. C., Rakich, J. V., and Tannehill, J. C., "Calculation of Supersonic Viscous Flow over Delta Wings with Sharp Subsonic Leading Edges," AIAA Paper 78-1132, Seattle, Wash., July 1977.

[7]McRae, D. S., "The Conically Symmetric Navier-Stokes Equations: Numerical Solution for Hypersonic Cone Flow at High Angle of Attack," AFFDL-TR-76-139, March 1977.

[8]Baldwin, B. S. and Lomax, H., "Thin Layer Approximation and Algebraic Model for Separated Turbulent Flows," AIAA Paper 78-257, Huntsville, Ala., Jan. 1978.

[9]Steger, J. L., "Implicit Finite-Difference Simulation of Flow About Arbitrary Two-Dimensional Geometries," *AIAA Journal*, Vol. 16, July 1978, pp. 679-686.

[10]Beam, R. and Warming, R. F., "An Implicit Factored Scheme for the Compressible Navier-Stokes Equations," *AIAA Journal*, Vol. 16, April 1978, pp. 393-402.